

ESTIMATES OF POLARIZATION CHARACTERISTICS OF LIDAR SIGNAL FROM SEA WATER CONTAINING THE STRATIFIED INHOMOGENEITIES

M.M. Krekova, G.M. Krekov, V.S. Shamanaev, and I.E. Penner

*Institute of Atmospheric Optics,
Siberian Branch of the Russian Academy of Sciences, Tomsk
Received October 28, 1993*

This paper presents the results of numerical and experimental investigations concerning the effect of optical inhomogeneities of different origin on the polarization characteristics of lidar signal. It is shown that the use of polarized radiation increases the amount of information obtained from the experimental data. Numerical estimates have been made for a lidar operating at the wavelength $\lambda = 0.53 \mu\text{m}$. Field experiments in the region of the Barents Sea have been carried out at the same wavelength.

It is well known that the use of polarized radiation increases the capabilities of laser radar techniques by increasing the amount of information obtained about the state of a medium and its composition. Its use for sounding of natural water areas in the bathymetry problems and for detection of fish schools increases the reliability of the data obtained.^{1,2} But the interpretation of the experimental measurements made by means of a polarization lidar may be difficult. Thus in a number of measurements made by the MAKREL' lidar³ in the region of the Barents Sea, the extrema in the amplitude-temporal characteristic of the signal were not accompanied by changes of its polarization structure, or the dependence of the depolarization ratio $\delta(h)$ was more complex in character for monotonic behavior of the signal amplitude $I(h)$. Obviously the extrema in the depth behavior of the signal amplitude $I(h)$ are connected with the presence of the submerged inversion layers in which either the concentration of hydrosol particles or their composition changes. The inversion layers appear as a result of various hydrodynamic, chemical, and biological processes that determine the optical structure of water in the region of inversion. To use the additional information contained in polarization measurements, it is necessary to investigate preliminary the response of the polarization characteristics to variations of the optical properties in the inversion layers.

The above-indicated investigations can be carried out in the numerical experiment that makes it possible to change the optical-geometrical conditions and to analyze the role of different factors in the formation of the signal characteristics separately. The numerical experiment was carried out by the Monte Carlo method. The principles of the algorithmic implementation and its peculiarities were described in Refs. 4 and 5, so let us indicate only the main points that determine the boundary and initial conditions of the problem. Calculations were made for airborne lidar systems promising for application to monitoring of the pollution sources, obtaining the express information about the bio-optical state of the region, investigation of the optical structure of subsurface water layers, and so on.

The initial and boundary conditions correspond to the typical configuration of a monostatic lidar. The linearly polarized optical signal whose waveform was described by the δ -function was incident normally on a plane-parallel scattering layer. A source located in the

plane $Y = 0$ of the spatial $\mathbf{r}(x, y, z)$ and angular $\Omega(a, b, c)$ coordinates radiated isotropically within the given cone of directions $2\pi(1 - \cos\phi_s)$. A detector had the discrete set of the field-of-view angles $2\pi(1 - \cos\phi_d^i)$, $i = 1, 2, \dots, n$. A lidar system was at the distance H from the water surface. Simulation of the ensemble of trajectories yields the statistical estimate of the amplitude-temporal characteristics of the Stokes vector-parameter $\mathbf{F}(I, Q, U, V)$ in the vicinity of the given detector. Then the depolarization ratio $\delta = (I - Q)/(I + Q)$ of the radiation was determined. The modification of the local estimate of the signal⁶ was used for the construction of the algorithm taking into account the high asymmetry of the sea water scattering phase functions.

The optical properties of the atmosphere over the ocean were for haze M .⁷ In calculations the sea water was considered to be the multicomponent medium, so the extinction coefficient was determined as a sum of additive components:

$$\sigma_{\text{ext}} = \sigma_{\text{sw}} + \sigma_{\text{sh}} + \chi_w + C_{\text{ch}} \chi_{\text{ch}} + C_y \chi_y,$$

where σ_{sw} , χ_w , and σ_{sh} are the scattering and absorption coefficients of clear water and hydrosol, respectively; C_{ch} , C_y and χ_{ch} , χ_y are the concentrations and absorptance of chlorophyll and yellow pigment, respectively. According to Ref. 8, they were taken to be equal to $\chi_{\text{ch}} = 0.009 \text{ m}^2/\text{mg}$, $\chi_w = 0.0271 \text{ m}^{-1}$, $\chi_y = 0.022 \text{ m}^{-1}$, and $\sigma_{\text{sw}} = 0.0023 \text{ m}^{-1}$. The arrays of experimental data obtained in different water areas of the Pacific and Atlantic Oceans⁹ were used as scattering phase matrices. They are seemed to be most representative due to the large number of measurements. It should be noted that the behavior of the nonzero components of the scattering phase matrices measured in the sea water areas, for example, in the Baltic Sea,¹⁰ duplicates that of the scattering phase matrices measured in Ref. 9, whereas their elements are close in values.

The scattering properties were determined by the relative contribution of concentrations of large organic and small mineral particles. This resulted in variety of the scattering phase functions of the sea water. The scattering phase functions $g_i(0)$ (Fig. 1) used in calculations were measured experimentally and were borrowed from Refs. 11 and 12. Their choice reflects the actual range of variations

of the scattering phase functions. So, the scattering phase functions $g_3(\theta)$ and $g_4(\theta)$ are more characteristic of the open ocean water where the organic particle fraction predominates, and the functions $g_1(\theta)$ and $g_2(\theta)$ are more characteristic of the water with enhanced content of particles of mineral origin.

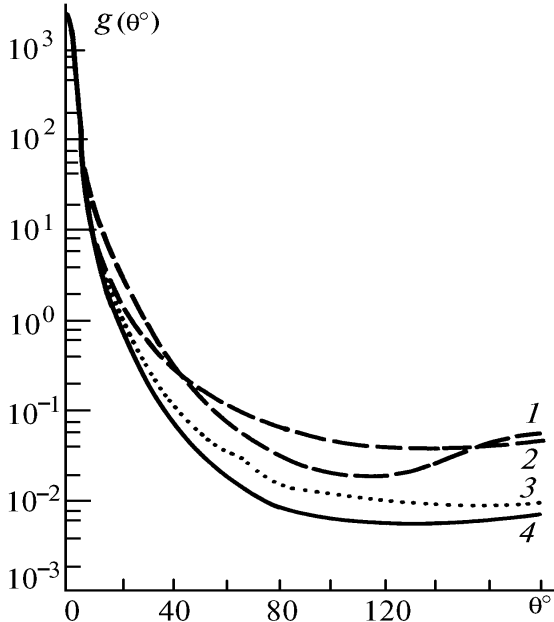


FIG. 1. Angular dependences of the scattering phase functions $g_1(\theta)$, ..., $g_4(\theta)$ indicated by the numbers adjacent to each curve.

Calculations were made for the wavelength $\lambda = 0.5 \mu\text{m}$, with the angular aperture of the source $1/2\varphi_s = 0.5 \text{ mrad}$ and the distance from the lidar to the ocean surface $H = 200 \text{ m}$.

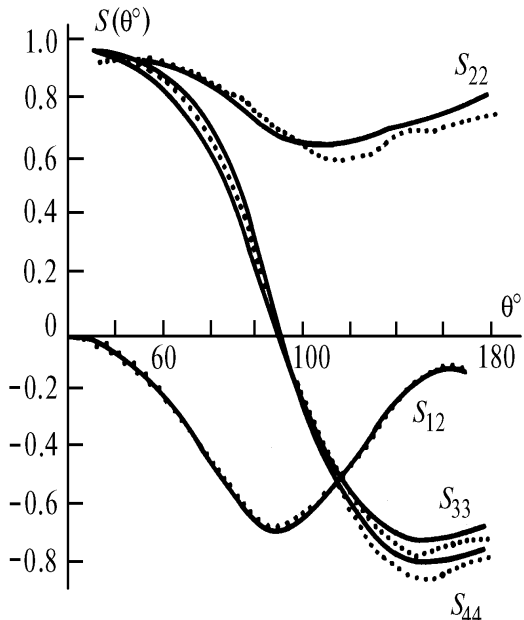


FIG. 2. Angular dependences of the normalized components of the model scattering phase matrices $S(\theta)$. S_1 is shown by solid lines, S_2 is shown by points.

Before we proceed to the discussion of the results of calculations of the polarization characteristics of the signal from the water containing inhomogeneities, we briefly describe the role of such key factors as the scattering phase matrix and the scattering phase function. Their angular dependences are shown in Figs. 1 and 2. It may be noted that the quantitative differences between the matrices $S_1(\theta)$ and $S_2(\theta)$ are in the limits $\sim 15\%$.

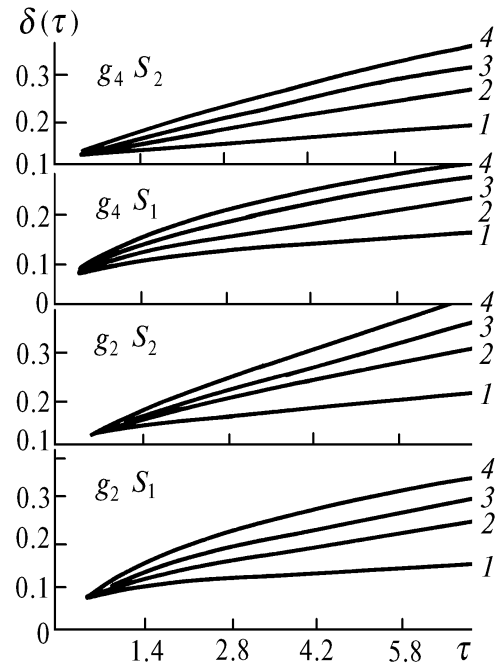


FIG. 3. Dependence of the depolarization ratio on the sounding depth for media that differ in their scattering properties. $\varphi_d = 5$ (1), 10 (2), 20 (3), and 35 mrad (4).

Figure 3 presents the results of calculation of the depolarization ratio $\delta(\tau)$ for the homogeneous composition of water with $\sigma_{\text{ext}}(h) = 0.22 \text{ m}^{-1}$. The results of calculations made for various types of water with different hydrosol composition are shown by corresponding families of curves. Numerical estimates show that small differences between the matrices $S_1(\theta)$ and $S_2(\theta)$ result in noticeable quantitative changes of the signal depolarization degree.

Let us compare the families of curves calculated for $g_4 S_1$ and $g_4 S_2$. The differences between the depolarization values of the total signal for two matrices $S_1(\theta)$ and $S_2(\theta)$ result from the difference between the depolarization ratio of the singly scattered signal δ_0 . Its values obtained from the results of calculations with the matrix S_1 is $\delta_0 = 0.08-0.09$, and with the matrix S_2 is $\delta_0 = 0.12-0.13$. The results shown in Fig. 3 as well as the data presented in Ref. 1 show that $\delta(h)$ has the neutral behavior for small receiving angles $\varphi_d \approx \varphi_s$. The stability under these conditions results from the low depolarization ratio of the background component of the signal $\delta_{bg}(h)$ being less than the value of depolarization of the singly scattered signal due to the fact that second-order scattering occurs at scattering angles θ close to π . The behavior of the scattering matrix components is quite stable at these scattering angles.

The shape of the scattering phase function also has a significant effect on the formation of the polarization

structure of the signal reflected from hydrosol. It is more pronounced under conditions of reception when $\varphi_d \gg \varphi_s$ and the multiple-scattering background is formed with the participation of photons of high multiplicity of scattering. This is confirmed by the results of calculation shown in Fig. 3. Let us compare the families of curves calculated with different values of φ_d for g_4S_1 and g_2S_1 as well as for g_4S_2 and g_2S_2 .

It should be noted that the effect of the shape of $g(\theta)$ on $\delta(h)$ is weakly pronounced for all observation angles j_d^i at optical depths $\tau \leq 1.5$ due to the fact that the return signal in this region is formed by photons with low multiplicities of scattering. The use of different combinations of the scattering phase matrices and the scattering phase functions in the calculations is caused by the lack of information about their correlation. This fact decreases somewhat the significance of quantitative estimates but is no bar to the qualitative analysis.

Previously in Ref. 13 we have considered the effect of the inhomogeneities engendered by the variations of the hydrosol concentration on the formation of the laser radar signal and its polarization characteristics. It has been shown that the sensitivity of the depolarization ratio to the extinction coefficient profile is weakly pronounced at small receiving angles, since the radiation with low multiplicities of scattering is concentrated in the viewing cone. The effect of the shape of the profile of $\sigma_{ext}(h)$ on $\delta(h)$ intensities with the increase of the receiving angles due to the fact that the radiation scattered at larger angles with higher degree of depolarization is added to the reflected signal. An analysis of the results of calculations shows that inversion of the optical density of the medium is accompanied by the coordinated appearance of maxima in the amplitude-temporal characteristic of the signal $I(h)$ and its depolarization $\delta(h)$ under appropriate optical-geometrical conditions of observation.

Interpretation of the results becomes much more difficult when the stratified inversion layers, that differ from the bulk of water in the composition of suspension, appear in the path of a beam. In this case the scattering properties of the medium change, that is, first of all the quantitative and qualitative characteristics of the scattering phase function change. Below we consider a number of possible submerged optical inversions.

The calculated results for $\sigma_{ext}(h) = \text{const} = 0.22 \text{ m}^{-1}$ at any depth is shown in Fig. 4 by curves 1 and 2. Only the composition of suspension was changed within the inversion layer with the thickness $\Delta h = 10 \text{ m}$ located at the depth $h = 10 \text{ m}$. The scattering properties of water within the layer largely composed of particles of mineral origin were described by the function $g_1(\theta)$ and outside the inversion — by the function $g_4(\theta)$. The maximum in the waveform of the signal $I(h)$ is caused only by the increase of the backscattering coefficient in the inversion zone determined by the shape of $g_2(\theta)$. Comparing the values of $\delta(h)$ calculated for this case with the results obtained for water with homogeneous composition, it may be noted that no peculiarities are observed in the behavior of $\delta(h)$. Qualitative character of the behavior of $\delta(h)$ remains the same as the receiving angles change.

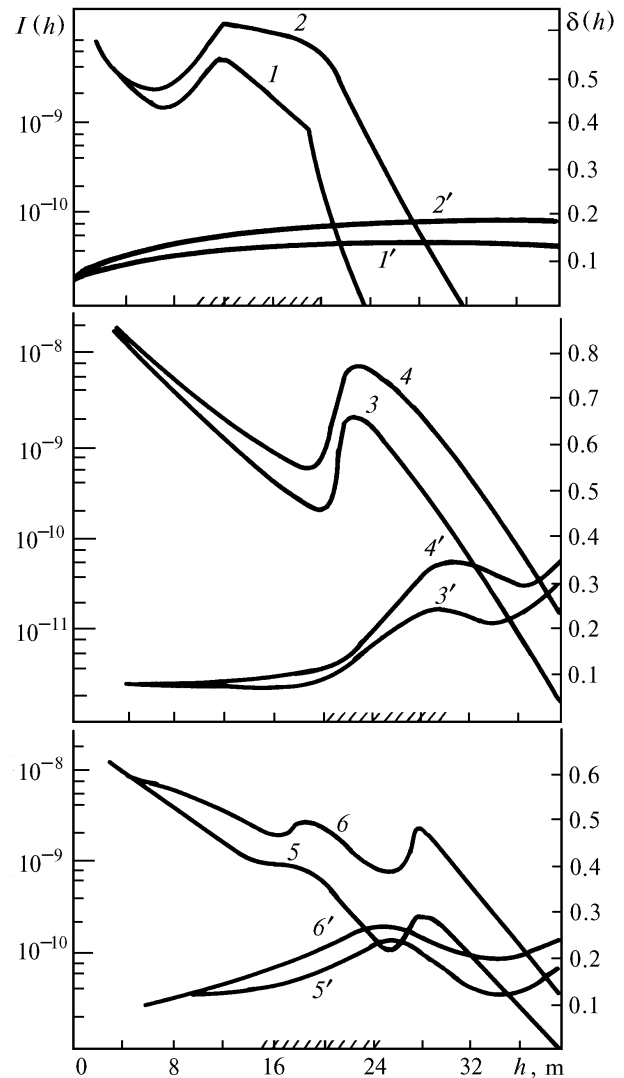


FIG. 4. Dependences of $I(h)$ (curves 1–6) and $\delta(h)$ (curves 1'–6') in the presence of the submerged inversion layers with different stratification. $\varphi_d = 5$ (1, 3, and 5) and 10 mrad (2, 4, and 6).

Curves 2 and 3 in this figure are for another optical situation in the presence of the hydrosol inversion layer with variable concentration of particles and suspension composition at the depth $h = 20 \text{ m}$. It was assumed that the extinction coefficient within the layer was equal to $\sigma_{ext}(h) = 0.6 \text{ m}^{-1}$, and the scattering properties were described by the function $g_2(\theta)$. Outside the layer, $\sigma_{ext}(h) = 0.18 \text{ m}^{-1}$ and the scattering phase function was $g_4(\theta)$. Such an optical situation may be caused by water carried out from rivers to the sea.

Enhanced content of the particles of mineral origin and less asymmetric scattering phase function (of g_1 and g_2 type shown in Fig. 1) are characteristic of this type of water mass. A strong spike is seen in the waveform $I(h)$. It is caused both by the abrupt change of the optical density of the medium and by the increase of the contribution of

scattered radiation at radar angles determined by the shape of $g_2(\theta)$. The polarization structure of the signal also changes. It is characterized by a rapid increase of the depolarization ratio $\delta(h)$ in the region of inversion. Outside the inversion, the slight decrease of $\delta(h)$ occurs due to the sharp decrease of the extinction coefficient. The growth of $\delta(h)$ in the inversion layer is more rapid than in the case in which only the concentration of suspension changes in the inversion zone¹⁰ (Fig. 4). It is connected with less asymmetric scattering phase function $g_2(\theta)$ resulting in the increase of depolarization of the background signal component $\delta_{bg}(h)$.

The results of calculations shown by curves 5 and 6 illustrate another possible optical situation, in which the appearance of the inversion layer of high optical density is caused by the biological processes. This may be the layer of phytoplankton with enhanced concentration of relatively large organic particles. This layer is characterized by highly asymmetric scattering phase function of the $g_4(\theta)$ type. The inversion layer with thickness $\Delta h = 10$ m was located at the depth $h_0 = 15$ m, in the layer $\sigma_{ext}(h) = 0.55 \text{ m}^{-1}$, outside it $\sigma_{ext}(h) = 0.20 \text{ m}^{-1}$, and the scattering phase function was $g_2(\theta)$.

Two maxima are seen in the waveform of the signal. The first maximum is caused by the abrupt change of the medium density, whereas the second maximum is caused by the change of the scattering properties of the medium outside of the inversion layer. The first maximum may be weakly pronounced due to the fact that the increase of the optical density in the layer is compensated by the decrease of the backscattering coefficient determined by $g(\pi)$. The depolarization ratio of the signal $\delta(h)$ sharply increases in the inversion zone, decreases outside of it, and then increases again due to the background component of the signal. The second maximum in $I(h)$ is in the region of decrease of $\delta(h)$.

A number of numerical estimates partially illustrated by the data shown in Fig. 4 show that the appearance of the extremum in the amplitude-temporal characteristic of the signal caused only by the change of the scattering properties of the medium is not accompanied by the extrema in its polarization structure.

The results of the aforementioned numerical experiments are in agreement with the data of field experiments shown in Fig. 5. The experiment was carried out over the Barents Sea by means of the MAKREL' airborne polarization lidar whose specifications were given in Ref. 3. The lidar was placed onboard the aircraft, the flight altitude was approximately 200 m, the angular divergence of the source was $\varphi_s = 1 \text{ mrad}$, the field-of-view angle was $\varphi_d = 13 \text{ mrad}$. Below we analyze the experiments in which the behavior of linear I_l and crosspolarized I_r components of the return signal had some peculiarities. In a number of measurements we observed the coordinated appearance of the maxima in the signal components. One of realizations is shown by curves 1 and 2 in Fig. 5 that illustrate the behavior of the amplitude-temporal characteristic of the signal $I(h) = I_l(h) + I_r(h)$ and its depolarization ratio $\delta(h) = I_r(h)/I_l(h)$. Based on the theoretical estimates,¹³ in this case the presence of the inversion layer with enhanced suspension concentration may be suggested at the depth $h = 12 \text{ m}$.

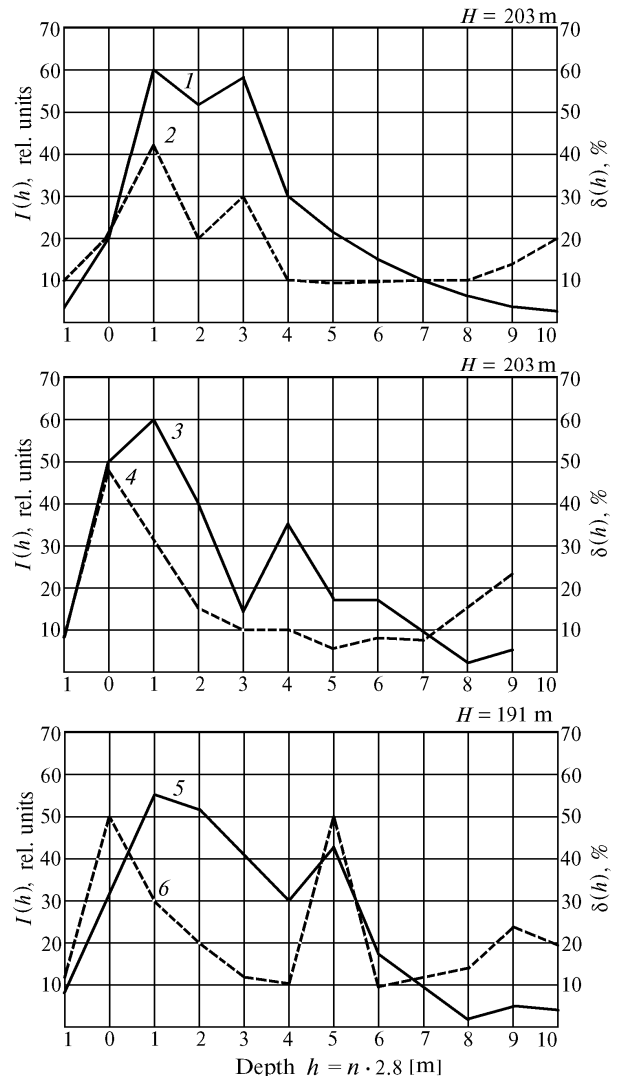


FIG. 5. Experimentally measured dependences of $I(h)$ and $\delta(h)$ for different regions of the Barents Sea. $I(h)$ is illustrated by solid curve and $\delta(h)$ — by dashed curve.

The next measurement run is illustrated by realization shown by curves 3 and 4 in Fig. 5. The extremum in the amplitude-temporal characteristic of the signal $I(h)$ points to the presence of the inversion layer at the depth $h = 18 \text{ m}$. At the same time, the characteristic $\delta(h)$ has no noticeable peculiarities. According to our estimates, such behavior of $I(h)$ and $\delta(h)$ may be due to relatively high content of particles of mineral fraction in the inversion layer, whereas the profile $\sigma_{ext}(h)$ remains practically unchanged at these depths. This assumption is in agreement with the data of numerical estimates illustrated by curves 1 and 2 in Fig. 4.

Curves 5 and 6 in Fig. 5 illustrate a run of measurements in another region of the sea. Maxima in the characteristics $I(h)$ and $\delta(h)$ indicate the presence of the inversion layer at the depth $h \approx 13-15 \text{ m}$. Large value of signal depolarization in the inversion zone points to the significant increase in the hydrosol particle concentration in this layer, and therefore in $\sigma_{ext}(h)$. But more weakly

pronounced maximum in $I(h)$ disagrees with sharp increase in $\sigma_{\text{ext}}(h)$. The discrepancy of mutual behavior of $I(h)$ and $\delta(h)$ will be removed if we suppose that both the concentration and the fraction composition of particles change in the inversion layer. The abrupt change of the optical density is compensated by the decrease of the portion of the backscattered radiation that is characteristic of water with dominant organic particle fraction (scattering phase function g_4 in Fig. 1), whereas the particles of mineral origin primarily determine the optical properties of water mass. This assumption is in agreement with the numerical estimates illustrated by curves 5 and 6 in Fig. 4.

Obviously for lack of simultaneous measurements of all components of the scattering phase matrices for different types of water the proposed analysis of the results of field measurements can be considered as an illustration of the fact that the amount of useful information obtained from lidar measurements can be increased.

It should be also noted that in our opinion, the use of the polarized radiation is more justified in laser sounding of the subsurface water layer in order to obtain the information about its optical properties. The analysis of both components of the signal makes it possible to avoid the erroneous interpretation of the results in the presence of submerged stratified inhomogeneities of different origin.

REFERENCES

1. I.E. Penner and V.S. Shamanaev, *Atmos. and Oceanic Opt.* **6**, No. 1, 65–67 (1993).
2. A.P. Vasil'kov, T.V. Kondranin, and E.V. Myasnikov, *Izv. Akad. Nauk SSSR, Fiz. Atmos. Okeana* **24**, No. 8, 873–881 (1988).
3. A.I. Abramochkin, V.V. Zanin, I.E. Penner, et al., *Opt. Atmos.* **1**, No. 2, 92–94 (1988).
4. V.E. Zuev, G.M. Krekov, and M.M. Krekova, *Izv. Akad. Nauk SSSR, Fiz. Atmos. Okeana* **19**, No. 6, 595 (1988).
5. G.I. Marchuk, G.A. Mikhailov, et al., *Monte Carlo Method in Atmospheric Optics* (Nauka, Novosibirsk, 1976), 284 pp.
6. V.V. Belov, G.M. Krekov, and G.A. Titov, in: *Problems of Remote Sensing of the Atmosphere* (Tomsk Affiliate of the Siberian Branch of the Academy of Sciences of the USSR, Tomsk, 1975), pp. 102–103.
7. D. Deirmendjian, *Electromagnetic Scattering on Spherical Polydispersions* (American Elsevier Publishing Company, Inc., New-York, 1969).
8. V.A. Urdenko and G. Tsimerman, ed., *Remote Sensing of Sea Taking into Account the Atmosphere* (Space Research Institute, Academy of Sciences of the German Democratic Republic, 1985), 272 pp.
9. K.J. Voss and E.S. Fry, *Appl. Opt.* **23**, No. 23, 4427 (1984).
10. E.A. Kadyshevich, *Izv. Akad. Nauk SSSR, Fiz. Atmos. Okeana* **13**, No. 1, 108 (1977).
11. G. Kullenberg, *Dep. Sea Res.* **15**, 423 (1968).
12. O.V. Kopelevich, "Optical properties of sea water," Doctoral Thesis in Phys. Math. Sciences, Moscow (1987).
13. G.M. Krekova and M.M. Krekova, *Atm. Opt.* **2**, No. 1, 55–61 (1989).